Mon. Not. R. Astron. Soc. **000**, 1–?? (2002) Printed 15 December 2012 (MN LaTeX style file v2.2)

A large sample of calibration stars for Gaia: $\log g$ from *Kepler* and CoRoT fields

O. L. Creevey[1⋆], F. Thévenin[1], S. Basu[2], W. J. Chaplin[3], L. Bigot[1], Mario. J. P. F. G. Mo

[1] *Laboratoire Lagrange, CNRS, Université de Nice Sophia-Antipolis, Nice, 06300, France.*
[2] *Department of Astronomy, Yale University, P.O. Box 208101, New Haven, CT 06520-8101, USA.*
[3] *School of Physics and Astronomy, University of Birmingham, Edgbaston, Birmingham B15 2TT, UK.*
[4] *Centro de Astrofísica and Faculdade de Ciências, Universidade do Porto, 4150-762 Porto, Portugal*
[5] *Institute of Space Sciences (CSIC-IEEC), Campus UAB, Facultad de Ciencias, Torre C5, parell 2, Bellaterra, Spain.*

Accepted sometime

ABSTRACT

Asteroseismic data can be used to determine stellar surface gravities with precisions of < 0.05 dex by using the *global seismic quantites* $\langle\Delta\nu\rangle$ and $\nu_{\max}$ along with standard atmospheric data such as $T_{\rm eff}$ and metallicity. Surface gravity is also one of the *four* stellar properties to be derived by automatic analyses for 1 billion stars from Gaia data (workpackage `GSP_Phot`). In this paper we explore seismic data from main sequence F, G, K stars (*solar-like stars*) observed by the *Kepler* spacecraft as a potential calibration source for the methods that Gaia will use for object characterisation ($\log g$). We compile a list of bright nearby stars for which radii and masses are known (e.g. from interferometry or binaries), and we compare their $\log g$ with those derived from asteroseismic data using a grid-based method. Agreement to within 1σ of the accepted $\log g$ values validates our method. We also find that errors in adopted atmospheric parameters (mainly [Fe/H]) can, however, cause systematic errors on the order of 0.02 dex. We then apply our method to a list of 41 stars to deliver precise values of surface gravity, and we find agreement with recent literature values. Finally we explore the typical precision that we expect in a sample of 400+ *Kepler* stars which have their global seismic quantities measured. We find typical uncertainties (precision) on the order of better than 0.02 dex in $\log g$. We study sources of systematic errors in $\log g$ and we find possible biases on the order of 0.04 dex in $\log g$ which accounts for errors in the $T_{\rm eff}$ and [Fe/H] measurements, as well as from using a different grid-based method. We conclude that *Kepler* stars provide a wealth of reliable information that can help to calibrate methods that Gaia will use, in particular, for source characterisation where excellent precision and accuracy in $\log g$ is obtained from *Kepler* data and this is one of the four stellar parameters to be extracted by `GSP_Phot`.

Key words: stars: fundamental parameters – stars: solar-type – surveys: Gaia – surveys: *Kepler* – Galaxy: fundamental parameters

1 INTRODUCTION

Large-scale surveys provide a necessary homogenous set of data for addressing key scientific questions. Their science-driven objectives naturally determine the type of observations that will be collected. However, to fully exploit the survey, complementary data, either of the same type but measured with a different instrument or of a different observable, needs to be obtained. Combining data from several large-scale surveys can only result in the best exploitation of both types of data.

The ESA Gaia mission[1] is due to launch in Autumn 2013. Its primary objective is to perform a 6-D mapping of the Galaxy (3 positional and 3 velocity data)[2] by observing over 1 billion stars down to a magnitude of $V = 20$. The mission will yield distances to these stars, and for about

⋆ E-mail:ocreevey@oca.eu

[1] http://sci.esa.int/science-e/www/area/index.cfm?fareaid=26
[2] For stars fainter than V∼11, the radial velocities will not be available.

20/100 million stars distances with precisions of less than 1%/10% will be obtained.

Gaia will obtain its astrometry by using broad band G photometry[3]. The spacecraft is also equipped with a spectrophotometer comprising both a blue and a red prism BP/RP, delivering *colour* information. A spectrometer will be used to determine the radial velocities of objects as far as $G = 17$ (typical precisions range from 1–20 kms^{-1}), and for the brighter stars ($G < 11$) high resolution spectra (R$\sim$11,500) will be available.

One of the main workpackages devoted to source characterisation is `GSP_Phot` whose objectives are to obtain stellar properties for 1 billion single stars by using the G band photometry, the parallax π, and the spectrophotometric information BP/RP (Bailer-Jones 2010). The stellar properties that will be derived are effective temperature $T_{\rm eff}$, surface gravity $\log g$, and metallicity [Fe/H], and also extinction $A_{\rm G}$ in the astrometric G band to each of the stars. Liu et al. (2012) discuss several different methods that were developed to determine these parameters using Gaia data and we refer to this paper and references within for details. In brief, they discuss the reliability of determining the four stellar parameters by using simulations, and in particular, they conclude that they expect typical precisions in the parameter $\log g$ on the order of 0.1 - 0.2 dex for main sequence late-type stars, with mean absolute residuals (direct value minus inferred value from simulations) no less than 0.1 dex for stars of all magnitudes, see Figure 14 and 15 of Liu et al. (2012). We note that the stellar properties derived by `GSP_Phot` will be used as initial input parameters for the workpackage devoted to detailed spectroscopic analysis of the brighter targets `GSP_Spec` (Recio-Blanco et al. 2006; Bijaoui et al. 2010; Worley et al. 2012) using the Radial Velocity Spectrometer data (Katz 2005). Spectroscopic determinations of $\log g$, $T_{\rm eff}$ and [Fe/H] are known to be subject to large correlation errors, which can severely inhibit the determination of chemical abundances.

The different algorithms discussed by Liu et al. (2012) used to determine the stellar properties in an automatic way have naturally been tested on synthetic data. However, to ensure the validity of the stellar properties, a set of 40 bright benchmark stars have been compiled and work is still currently underway to derive stellar properties for all of these in the most precise, homogenous manner (e.g. Heiter, et al. in prep.). Unfortunately, these benchmark stars will be too bright for Gaia, and so a list of about 500 primary reference stars has also been compiled. The idea is to use precise ground-based data and the most up-to-date models (known from working with the benchmark stars) to determine their stellar properties as accurately and precisely as possible. These primary reference stars will be observed by Gaia and thus will serve as a set of calibration stars. A third list of secondary reference stars has also been compiled. These consist of about 5000 fainter targets.

In the last decade or so, much progress in the field of asteroseismology has been made, especially for stars exhibiting Sun-like oscillations. These stars have deep outer convective envelopes where stochastic turbulence gives rise to a broad spectrum of excited resonant oscillation modes (e.g. Ulrich 1970, Leibacher & Stein 1971, Brown & Gilliland 1994, Figs. 2 of Salabert et al. 2002, Bouchy & Carrier 2002). The power spectrum of such stars can be characterised by some global seismic quantities; $\langle\Delta\nu\rangle$, $\nu_{\rm max}$, and $\langle\delta\nu\rangle$. The quantity $\langle\Delta\nu\rangle$ is the mean value of the *large frequency separations* $\Delta\nu_{l,n} = \nu_{l,n} - \nu_{l,n-1}$ where $\nu_{l,n}$ is a resonant oscillation frequency with degree l and radial order n, $\nu_{\rm max}$ is the frequency corresponding to the maximum amplitude of the bell-shaped frequency spectrum, and $\langle\delta\nu\rangle$ is the mean value of the *small frequency separations* $\delta\nu_{l,n} = \nu_{l,n} - \nu_{l+2,n-1}$.

Even when individual frequencies can not be determined from the frequency spectra both $\langle\Delta\nu\rangle$ and $\nu_{\rm max}$ can still be extracted quite robustely (see e.g. Verner et al. 2011 and references therein), and these have been shown to scale with stellar parameters such as mass, radius, and $T_{\rm eff}$ e.g. Brown & Gilliland (1994); Bedding & Kjeldsen (2003); Stello et al. (2008); Huber et al. (2011); Bedding (2011); Miglio et al. (2012); Silva Aguirre et al. (2012). By comparing the theoretical seismic quantities with the observed ones over a large grid of stellar models, very precise determinations of $\log g$ (< 0.03 dex) and mean density ($< 2\%$) can be obtained for main sequence F, G, K stars (Bruntt et al. 2010; Metcalfe et al. 2010; Gai et al. 2011; Mathur et al. 2012; Creevey et al. 2012a).

Of particular interest for Gaia is the *Kepler*[4] field of view, $\sim$100 square-degrees, centered on galactic coordinates 76.32°, +13.5°. *Kepler* is a NASA mission dedicated to characterising planet-habitability (Borucki et al. 2010). It obtains photometric data of approximately 150,000 stars with a typical cadence of 30 minutes. However, a subset of stars (less than 1000 every month) acquire high-cadence data with a point every 1 minute. This is sufficient to detect and characterise Sun-like oscillations in many stars. Verner et al. (2011) and Chaplin et al. (2011) recently showed the detections of the global seismic quantities for a sample of 600 F, G, K main sequence and subgiant (V/IV) stars with typical magnitudes $7 < V < 12$, while both CoRoT and *Kepler* have both shown their capabilities of detecting these same seismic quantities in 1000s of red giants, e.g. Hekker et al. (2009); Kallinger et al. (2010); Bedding et al. (2010); Baudin et al. (2011); Mosser et al. (2012).

With the detection of the global seismic quantities in hundreds of main sequence stars, the *Kepler* field is very promising for helping to calibrate Gaia `GSP_Phot` methods. In particular, the global seismic quantities deliver one of the four properties to be extracted by automatic analysis, namely $\log g$. Recently, Gai et al. (2011) studied the distribution of errors for a sample of simulated stars using seismic data and a grid-based method based on stellar evolution models. They concluded that $\log g$ derived from seismic properties (*"seismic* $\log g$*"*) is almost fully independent of the input physics in the stellar evolution models that are used. More recently Morel & Miglio (2012) compared classical determinations of $\log g$ to those derived alone from a scaling relation (see Eq.[2]), and concluded that the mean differences between the various methods used is $\sim$0.05 dex, thus supporting the validity of a seismic determination of

[3] The photometric scales of G and the usual V band are very similar.

[4] `http://kepler.nasa.gov`

$\log g$. While some studies have focussed on comparing values of radii or masses using different methods, for example, Bruntt et al. (2010), no study has been done focussing on both the *accuracy and precision* of a seismic $\log g$ using one or more grid-based methods for stars with accurately measured radii *and* masses. The accuracy and precision in $\log g$ for these bright stars has also not been tested while considering precisions in data such as those obtained by *Kepler*. Such a study could validate the use of seismic data as a calibration source for Gaia.

With these issues in mind, the objectives of this paper are to (i) test the accuracy of a seismic $\log g$ from a grid-based method using bright nearby targets for which radii and masses have been measured (Sect. 3), (ii) determine $\log g$ for an extended list of stars whose global seismic properties and atmospheric parameters are available in the literature (Sect. 4) using the validated method, and (iii) study the distribution of $\log g$ and their uncertainties of over 400 *Kepler* stars as derived by grid-based methods while concluding on realistic precisions and systematic errors for this potential sample of Gaia calibration stars (Sect. 5). We begin in Sect. 2 by summarising the different methods available for determining $\log g$.

2 DIRECT METHODS TO DETERMINE $\log g$

In this section we summarise the various methods that are used to determine the surface gravity (or the logarithm of this $\log g$) of a star. Comparing each of these methods directly would be the ideal approach for unveiling shortcomings in our models (systematic errors) and reducing uncertainties while also increasing accuracy by de-coupling stellar parameters.

2.1 Derivation of $\log g$ from independent determinations of mass and radius

The most direct method of determining $\log g$ involves measuring the mass M and radius R of a star in an independent manner. g is calculated using Newton's Law of Gravitation: $g = GM/R^2$ where G is the gravitational constant.

2.1.1 Mass and radius from eclipsing binary systems

For detached eclipsing spectroscopic binaries, both M and R can be directly measured by combining photometric and radial velocity time series (Ribas et al. 2005; Creevey et al. 2005, 2011; Hełminiak et al. 2012). The orbital solution is sensitive to the mass ratio and the individual $M \sin i$ of both components, where i is the inclination. The photometric time series displays eclipses (when the orbital plane has a high enough inclination) that are sensitive to i and the relative R. Once i is derived, then the individual M are solved. Kepler's Law relates the orbital period of the system Π, the system's M, and the separation of the components. Π is known from either eclipse timings or observing a full radial velocity orbit. Once the individual M are known then Π scales the system (providing the separation) and thus the individual R. g is then calculated using Newton's Law.

2.1.2 Mass and radius from interferometry and asteroseismology

R is measured by combining the angular diameter θ as measured from interferometry with the distance to the star. The distance (or its inverse the parallax) has been made available using data from the Hipparcos satellite for stars with $V\ <\sim\ 8$ mag (Perryman et al. 1997; van Leeuwen 2007; Kervella et al. 2003). Indirect methods also exist for determining the angular diameter of a star, such as combining $T_{\rm eff}$ with measurements of bolometric flux (Silva Aguirre et al. 2012), or from calibrated relations using photometry (Kervella et al. 2004). Once R is known, then a model-independent mass determination can be obtained by using the asteroseismic relation which links mean density $\langle\rho\rangle$ and $\langle\Delta\nu\rangle$;

$$\frac{\langle\Delta\nu\rangle}{\langle\Delta\nu\rangle_\odot} \approx \sqrt{\frac{\rho}{\rho_\odot}} = \sqrt{(M/M_\odot)/(R/R_\odot)^3} \qquad (1)$$

where $\langle\Delta\nu\rangle_\odot$ is the solar value (e.g. Kjeldsen & Bedding 1995; Huber et al. 2011).

2.1.3 Asteroseismic mass

When high signal-to-noise ratio seismic data are available, individual oscillation frequencies can be used to do detailed modelling, and hence determine M (e.g. Doğan et al. 2010; Brandão et al. 2011; Bigot et al. 2011; Metcalfe et al. 2012a; Miglio et al. 2012a). However, this method depends on the physics in the interior stellar models unlike the methods mentioned earlier, and using different input physics may result in different values of mass. Typical uncertainties/accuracies in such a value does not usually exceed about 5% for bright targets, which translates to less than a 0.02 dex error in $\log g$ for stars that we consider in this work. When combined with an independently measured radius, the mass uncertainties can reduce to $< 3\%$ (Creevey et al. 2007; Bazot et al. 2011; Huber et al. 2012).

2.2 Spectroscopic determinations of $\log g$

The surface gravity of a star is usually derived from an atmospheric study with spectroscopic data (e.g. Thévenin & Jasniewicz 1992; Bruntt et al. 2010; Lebzelter et al. 2012; Sousa et al. 2012). There are two usual approaches for deriving atmospheric parameters ($\log g$, $T_{\rm eff}$, and [Fe/H]). The first approach is based on directly comparing a library of synthetic spectra with the observed one, usually in the form of a best-fitting approach. A major shortcoming of this approach is that combinations of parameters can produce similar synthetic spectra so that many correlations between the derived parameters exist. The more classical method for determining atmospheric parameters relies on measuring the equivalent widths of iron lines (or other chemical species). This method assumes local thermodynamic equilibrium (LTE) and requires model atmospheres. Once the $T_{\rm eff}$ is determined (by requiring that the final line abundance is independent of the excitation potential or for stars with $T_{\rm eff} > 5000$ K, measuring the Balmer H line profiles), then g is the only parameter controlling the ionisation balance of a chemical element in the photospheric layers, which acts on the recombination frequency of electrons and ions. g is then determined by requiring a balance between different ionized lines e.g. Fe-I and Fe-II. Spectroscopically determined $\log g$ can have large systematic errors especially for more metal-poor stars where NLTE effects must be taken into account. This can change $\log g$ by $\sim$0.5 dex, e.g. Thévenin & Jasniewicz (1992).

2.3 $\log g$ derived from Hipparcos data

An alternative method for determining $\log g$ relies on knowing the distance d to the star from astrometry, its bolometric flux (combining these gives the luminosity of a star) and the effective temperature $T_{\rm eff}$. Then substituting M and $\log g$ for R in Stefan's Law, one obtains the following $\log g = 10.537 - \log M - 0.4(V_0 + {\rm BC}) + 2\log d - 4\log T_{\rm eff}$, where V_0 is the de-reddened V magnitude and BC$_V$ the bolometric correction in V, and M is estimated from evolution models, for example Thévenin et al. 2001; Barbuy et al. 2003). This *Hipparcos* $\log g$ is often used as a fixed parameter for abundance analyses of stars. Typical uncertainties are no less than 0.08 dex where especially M is usually not well known, and errors from d and $T_{\rm eff}$ are not insignificant. We note that Gaia will deliver unmistakeably accurate distances for much fainter stars and these will provide an alternative $\log g$ for such stars.

2.4 $\log g$ from evolutionary tracks

2.4.1 Classical constraints in the HR diagram

When H-R diagram constraints are available ($T_{\rm eff}$, L, metallicity) then the stellar evolution tracks can be used to provide estimates of some of the other parameters of the star, e.g. mass, radius, and age. While correlations exist between many parameters, e.g. mass and age, these correlations also allow us to derive certain information with better precision, e.g. mass and radius gives g. By exploring a range of models that pass through the error box thus allows us to limit the possible range in $\log g$ (e.g. Creevey et al. 2012b).

2.4.2 Grid-based asteroseismic $\log g$

Apart from performing detailed modelling using asteroseismic data, one can rely on grids of stellar models to estimate stellar properties such as mass and radius with precisions on the order of 2–10%. However, because asteroseismic data are extremely sensitive to the ratio of these two parameters, then very precise determinations of $\log g$ and $\langle\rho\rangle$ can be obtained in an almost model-independent manner (Gai et al. 2011). (In Sect. 5.3 we address this issue). Such a *grid-based asteroseismic* $\log g$ can be obtained in the following manner: a large grid of stellar models that spans a wide range of mass, age, and metallicity is constructed. Each model with a given mass, age, and chemical composition has a corresponding set of theoretical observables, such as R, $\log g$, and $T_{\rm eff}$, including individual frequencies, $\langle\Delta\nu\rangle$ and $\nu_{\rm max}$. Eq. 1 can be used to calcualate $\langle\Delta\nu\rangle$ or it can be calculated directly from the oscillation frequencies derived from the structure model. The amplitudes of oscillation modes, however, are much more difficult to predict and the empirical relation for $\nu_{\rm max}$ is the standard scaling relation used:

$$\frac{\nu_{\rm max}}{\nu_{\rm max,\odot}} \approx \frac{(M/M_\odot)}{(R/R_\odot)^2\sqrt{T_{\rm eff}/T_{\rm eff,\odot}}} \qquad (2)$$

where $\nu_{\rm max,\odot}$ is the solar value (e.g. Vandakurov 1968; Tassoul 1980; Kjeldsen & Bedding 1995). A set of input observed data, e.g. $\{\langle\Delta\nu\rangle$, $T_{\rm eff}$, and [Fe/H]$\}$, is compared to the theoretical ones, and the models that give the best match to the data are selected and the value of $\log g$ and its uncertainty is derived using these best selected models. Several such approaches have been discussed and applied in the recent literature (Stello et al. 2009; Quirion et al. 2010; Basu et al. 2010; Gai et al. 2011; Creevey et al. 2012a; Metcalfe et al. 2012a; Silva Aguirre et al. 2012) some of which use individual frequencies or Eq. 1 to calculate $\langle\Delta\nu\rangle$ and in Section 3 we detail the method used in this paper. For the rest of this paper we use the term *seismic* $\log g$ to refer specifically to the grid-based method for determining $\log g$.

3 COMPARISON OF DIRECT AND SEISMICALLY DETERMINED $\log g$.

3.1 Observations and direct determination of $\log g$

In order to test the reliability of an asteroseismically determined $\log g$, the most correct method is to compare it to $\log g$ derived from mass and radius measurements of stars in eclipsing binaries (Sect. 2.1.1) (apart from the Sun). Unfortunately the number of stars whose masses and radii are known from binaries, where seismic data are also available, is quite limited. For this sample of stars we have α Cen A and B, and Procyon. Following this, we rely on the combination of asteroseismology and interferometry to determine $\log g$, and using the scaling relation which relates density to the observed properties of $\langle\Delta\nu\rangle$ and R to provide an independent M measurement (Sect. 2.1.2). However, since this scaling relation is used explicitly in the grid-based method, we have opted to omit stars where this method provides the mass, except for the solar twin 18 Sco, which was included because of its similarity to the Sun. To complete the list of well-characterised stars we have then chosen some targets for which an interferometric R has been measured and detailed seismic modelling has been conducted to determine the star's M by several authors (Sect. 2.1.3). The stars which fall into this group are HD 49933 and β Hydri. The seven stars are listed in order of $\log g$ in Table 1 along with $\langle\Delta\nu\rangle$, $\nu_{\rm max}$, $T_{\rm eff}$, [Fe/H], M, and R. When several literature values are available these are also listed. The final column in the table gives the *direct* value of $\log g$ as derived from M and R. For HD 49933 and β Hydri we adopt the weighted mean value of $\log g$ which is 4.214 and 3.952 dex respectively (see Table 1). For the rest of the paper we refer to these determinations of $\log g$ as the *direct* determinations.

3.2 Seismic method to determine $\log g$

We use the grid-based method, RadEx10, to determine an asteroseismic value of $\log g$ (Creevey et al. 2012a). The grid was constructed using the ASTEC stellar evolution code (Christensen-Dalsgaard 2008) with the following configuration: the EFF equation of state (Eggleton et al. 1973) without Coulomb corrections, the OPAL opacities

Table 1. Properties of the reference stars

Star	$\langle\Delta\nu\rangle$ (μHz)	$\nu_{\rm max}$ (mHz)	$T_{\rm eff}$ (K)	[Fe/H] (dex)	R ($R_\odot$)	M ($M_\odot$)	$\log g$ (dex)
αCenB	161.5 ± 0.11[1a]	4.0[1a]	5316 ± 28[1b]	+0.25 ± 0.04[1b]	0.863 ± 0.005[1c]	0.934 ± 0.006[1d]	4.538 ± 0.008
					0.863 ± 0.003[1e]		
18 Sco	134.4 ± 0.3[2a]	3.1[2a]	5813 ± 21[2a]	0.04 ± 0.01[2a]	1.010 ± 0.009[2a]	1.02 ± 0.03[2a]	4.438 ± 0.005
Sun	134.9 ± 0.1[3a]	3.05[3b]	5778 ± 20[3c]	0.00 ± 0.01			4.437 ± 0.002[3d]
αCenA	105.6[4a]	2.3[4a] e	5847 ± 27[1b]	+0.24 ± 0.03[1b]	1.224 ± 0.003[1c]	1.105 ± 0.007[1d]	4.307 ± 0.005
		2.4[4b]					
HD 49933	85.66 ± 0.18[5a]	1.8[5a]	6500 ± 75[5b]	-0.35 ± 0.10[5b]	1.46 ± 0.05[5b]		4.24[5b]
		1.657 ± 0.028[5c]			1.49[5b]	1.325[5b]	4.22[5b]
			6640 ± 100[5d]	-0.38[5d]	1.42 ± 0.04[5d]	1.20 ± 0.08[5d]	4.212 ± 0.039
					1.39 ± 0.04[5e]	1.12 ± 0.03[5e]	4.201 ± 0.027
					1.44 ± 0.04[5e]	1.20 ± 0.03[5e]	4.200 ± 0.027
Procyon	55.5 ± 0.5[6a]	1.0[6b]	6530 ± 90[6c]	-0.05 ± 0.03[6d]	2.067 ± 0.028[6e]	1.497 ± 0.037[6f]	3.982 ± 0.016
βHydri	57.24 ± 0.16[7a]	1.0[7a]	5872 ± 44[7b]	-0.10 ± 0.07[7c]	1.814 ± 0.017[7b]	1.07 ± 0.03[7b]	3.950 ± 0.015
						1.04[7d]	3.938 ± 0.015
						1.082[7e]	3.955 ± 0.015
						$1.10^{+0.04}_{-0.07}$[7f]	3.962 ± 0.030
			5964 ± 70[7g]	0.03 ± +0.07[7g]	1.69 ± 0.05[7g]	1.17 ± 0.05[7g]	4.02 ± 0.04[7g]

References: [1a]Kjeldsen et al. (2005), [1b]Porto de Mello et al. (2008), [1c]Kervella et al. (2003), [1d]Pourbaix et al. (2002), [1e]Bigot et al. (2006), [2a]Bazot et al. (2011), [3a]Taking the average of Table 3 from Toutain & Froehlich (1992), [3b]Kjeldsen & Bedding (1995), [3c]Grevesse & Sauval (1998), [3d]$1M_\odot$=1.98919e30 kg, $1R_\odot$=6.9599e8 km, $G = 6.67384e11$ m^3 kg^{-1} s^{-2}(NIST database), [4a]Bouchy & Carrier (2002), [4b]Quirion et al. (2010), [5a]Using the $l = 0$ modes with Height/Noise>1 from Table 1 of Benomar et al. (2009), [5b]Kallinger et al. (2010) $Z = 0.008 \pm 0.002$ is referenced, [5c]Gruberbauer et al. (2009), [5d]Bigot et al. (2011), [5e]Creevey & Bazot (2011), [6a]Eggenberger et al. (2004), [6b]Martić et al. (2004), [6c]Fuhrmann et al. (1997), [6d]Allende Prieto et al. (2002), [6e]Kervella et al. (2004), [6f]Girard et al. (2000), [7a]Bedding et al. (2007), [7b]North et al. (2007), [7c]Bruntt et al. (2010), [7d]Brandão et al. (2011), [7e]Doğan et al. (2010), [7f]Fernandes & Monteiro (2003), [7g]da Silva et al. (2006)

(Iglesias & Rogers 1996) supplemented by Kurucz opacities at low temperatures, solar mixture from Grevesse & Noels (1993), nuclear reaction rates from Bahcall & Pinsonneault (1992). Convection in the outer convective envelope is described by the mixing-length theory of Böhm-Vitense (1958) and this is characterised by a variable parameter $\alpha_{\rm MLT}$ (where $l = \alpha_{\rm MLT} H_p$ l is the mixing-length and H_p the pressure scale height). When a convective core exists, there is an overshoot layer which is also characterised by the *conveccctive core overshoot parameter* $\alpha_{\rm ov}$ and this is set to 0.25 (an average of values used recently in the literature). Finally we ignore diffusion effects. For a correct determination of mass and age, diffusion is an important ingredient in stellar models.

The grid considers models with masses from 0.75 – 2.00 $M_\odot$. We calculate models with ages from ZAMS to subgiant, initial metallicity $Z_{\rm i}$ spans 0.003 – 0.030 in steps of ~ 0.003, while initial hydrogen abundance $X_{\rm i}$ is set to 0.71: this corresponds to an initial He abundance $Y_{\rm i} = 0.260 - 0.287$. The mixing length parameter $\alpha_{\rm MLT} = 2.0$ is used, which was obtained by calibrating it with solar data. We note that to derive other stellar properties, it is very important to allow $\alpha_{\rm MLT}$ to vary e.g. Creevey et al. (2012b); Bonaca et al. (2012).

To obtain the grid-based model stellar properties ($\log g$, M, R, luminosity L, t) we perturb the set of input observations using a random Gaussian distribution, and compare the perturbed observations to the model ones. In this method, $\langle\Delta\nu\rangle$ is calculated using Eq. 1. The input observations consist primarily of $\langle\Delta\nu\rangle$, $\nu_{\rm max}$, $T_{\rm eff}$, and [Fe/H], although other inputs are possible, for example, L or R. The stellar parameters and uncertainties are defined as the mean value of the fitted parameter from 10,000 realizations, with the standard deviations defining the 1σ uncertainties. In this work, we consider just the derived value of $\log g$.

3.3 Analysis approach

We determine a seismic $\log g$ for the reference stars using the method explained above. We consider different sets of input data in order to test how sensitive the different observations are to the accuracy (and precision) of a seismic $\log g$:

(S1) $\{\langle\Delta\nu\rangle$, $\nu_{\rm max}$, $T_{\rm eff}$, [Fe/H]$\}$,
(S2) $\{\langle\Delta\nu\rangle$, $\nu_{\rm max}$, $T_{\rm eff}\}$, and
(S3) $\{\langle\Delta\nu\rangle$, $T_{\rm eff}\}$,

For the potential sample of Gaia calibration stars, [Fe/H] will not always be available, and in some cases, $\nu_{\rm max}$ is difficult to detect for very low S/N detections.

The observational errors in our sample are very small due to the brightness and proximity of the star, so we also derive an asteroseismic $\log g$ while considering observational errors that we expect for *Kepler* stars (see Verner et al. 2011 and Figure 4). We consider three types of observational errors while repeating the exercise:

(E1) the true measurement errors from the literature,
(E2) typically "good" errors expected for these stars, i.e. $\sigma(\langle\Delta\nu\rangle) = 1.1$ μHz, $\sigma(\nu_{\rm max}) = 5\%$, $\sigma(T_{\rm eff}) = 70$ K, and σ([Fe/H]) = 0.08 dex (see Sect. 5.1), and

Table 2. $\log g$ derived by RadEx10 for the reference stars using the true measurement errors.

Star	$\log g$ (dex)	$\log g_{\rm direct}$ (dex)
α Cen B	4.527 $\pm$ 0.004	4.538
18 Sco	4.441 $\pm$ 0.004	4.438
Sun	4.438 $\pm$ 0.001	4.437
α Cen A	4.312 $\pm$ 0.004	4.307
HD 49933	4.195 $\pm$ 0.007	4.218
Procyon	3.981 $\pm$ 0.006	3.982
β Hydri	3.957 $\pm$ 0.010	3.952

(E3) "not-so-good" measurement errors, primarily considering the fainter targets (V∼11,12), i.e. $\sigma(\langle\Delta\nu\rangle)$ = 2.0 μHz, $\sigma(\nu_{\rm max})$ = 8%, $\sigma(T_{\rm eff})$ = 110 K, and σ([Fe/H]) = 0.12 dex.

3.4 Seismic versus direct $\log g$

In Figure 1 we compare the grid-based seismic $\log g$ with the direct $\log g$ for the seven stars. Each star is represented by a point on the abscissa, and the y-axis shows (seismic - direct) value of $\log g$. There are three panels which represent the results using the three sets of input data. We also show for each star in each panel three results; in the bottom left corner these are marked by 'E1', 'E2', and 'E3', and they represent the results using the different errors in the observations. The black dotted lines represent *seismic minus direct* $\log g$ = *0*, and the grey dotted lines indicate $\pm$0.01 dex.

Figure 1 shows that for all observational sets and errors $\log g$ is generally estimated to within 0.02 dex in both precision and accuracy. This result clearly shows the validity of the global seismic quantities and atmospheric parameters for providing an extremely precise value of $\log g$. Other general trends that can be seen are that the typical *precision* in $\log g$ decreases as (1) the observational errors increase (from E1 – E3), and (2) the information content decreases (S1 – S2 – S3, for example). One noticeable result is the systematic offset in the derivation of $\log g$ for HD 49933 when we use [Fe/H] as input (S1). This could be due to an incorrect metallicity, an error in the adopted direct $\log g$ or a shortcoming of the grid of models. This star shows stellar activity (Mosser et al. 2005; García et al. 2010; Salabert et al. 2011) and not including magnetic effects in stellar models will effect the determination of [Fe/H], e.g. Fabbian et al. (2012) and consequently the determination of other stellar parameters such as mass. The effect of magnetic fields on the seismic parameters has been shown to be smaller than the errors cite bigot. The typical spread in $\log g$ for this star as shown in Table 1 is about 0.02 dex which is also the size of the offset. However, this 0.02 dex offset is still much better than any spectroscopic determination of $\log g$. In Table 2 we summarize the derived value of $\log g$ and the direct value using S1 with the true observational errors (E1).

3.5 Systematic errors in observations

For all of the calculations we have assumed that the input observations are correct (accurate). While this is certainly more true for brighter nearby targets where high SNR data can be obtained, the same cannot be said for fainter stars. In particular with spectroscopic data, the determination of $T_{\rm eff}$ and [Fe/H] are correlated and depend on the analysis methods used and the different model atmospheres (see e.g. Creevey et al. 2012a; Lebzelter et al. 2012). Additionally for many stars a photometric temperature may be the only available one and while these estimates are very good, systematic errors are still unavoidable (Casagrande et al. 2010; Boyajian et al. 2012), in particular due to unknown reddenning, and larger photometric errors lead to larger errors on the temperatures. This is not only a problem for fainter stars. For example, for β Hydri we found two determinations of $T_{\rm eff}$ — an interferometric one and a spectroscopic one. Additionally, metallicities derived from spectroscopic data depend on the adopted $T_{\rm eff}$.

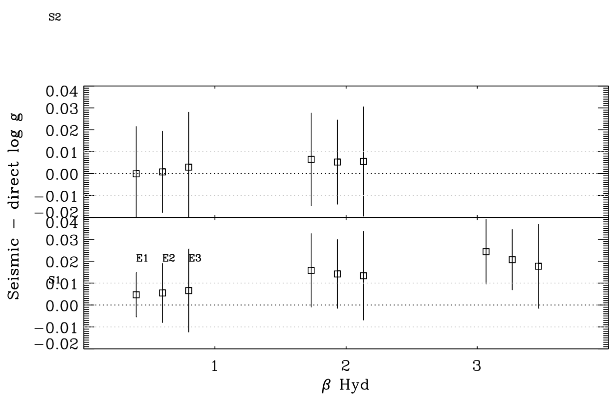

Figure 2. *Seismic-minus-direct* values of $\log g$ for β Hydri when the observations with systematic errors included for cases 2 and 3 are analysed by the seismic method.

To study the effect of *systematic errors* in the observations, we repeated our analysis for β Hydri while using three sets of input data that change only in $T_{\rm eff}$ and [Fe/H]. The first set (1) uses the values as given by North et al. (2007) (5872, –0.10), the second set (2) uses (5964, –0.10), and the third set (3) uses (5964, –0.03) as given by da Silva et al. (2006). The results for S1 and S2 are shown in Figure 2. The lower panel shows that for a systematic error in both $T_{\rm eff}$ and [Fe/H] the accuracy decreases. The top panel shows that when we only consider the $T_{\rm eff}$ information we get a smaller increase in the offset than when we consider both $T_{\rm eff}$ and [Fe/H]. One way of interpreting this result is by considering that in S2 there is much more weight assigned to the seismic data than the atmospheric data, and so an incorrect atmospheric parameter should not influence the final result as much as in case S1 where the atmospheric parameters have more weight. In the latter case, an incorrect $T_{\rm eff}$ with the correct [Fe/H] will necessarily shift the mass either up or down, and result in a more displaced $\log g$. However, in both cases, we see that the offset does not exceed 0.03 dex. For the radius and mass, however, a systematic error has a much more profound effect on the offset. In this case biases on the order of up to 6% and 20% in radius and mass can be obtained (Creevey & Thévenin 2012). It must also be noted that a systematic error in the atmospheric parameters is going to have a much larger negative effect when we use only the *global* seismic quantities instead of a performing a detailed seismic analysis with individual frequencies, where they have much more weight in the fitting process.

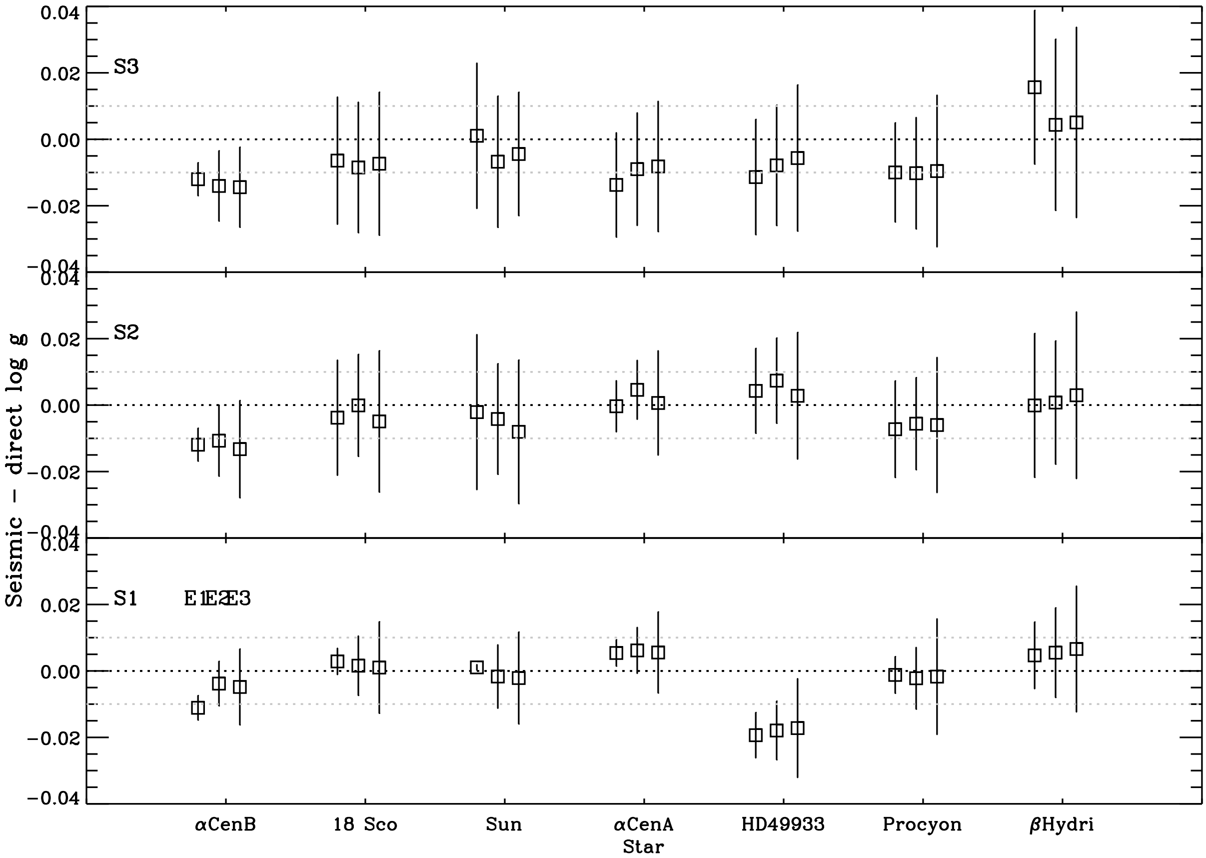

Figure 1. *Seismic-minus-direct* $\log g$ for the seven sample stars while considering different subsets of input observations (different panels) and different observational errors.

3.6 Seismic determination of $\log g$ from the global seismic quantities for the reference stars

We summarize $\log g$ for the sample stars in Table 2 derived by RadEx10 using $\langle\Delta\nu\rangle$, $\nu_{\rm max}$, $T_{\rm eff}$, and [Fe/H], and the true observational errors. We highlight the excellent agreement between our seismically determined parameters, and those obtained by direct mass and radius estimates. $\log g$ is matched to within 1σ (< 0.015 dex) for all stars. We must also comment on the very small uncertainties given in Table 2; these results were obtained using the true (very small) observational errors given in Table 1 and typically one would not expect to obtain such small errors. As can be seen, the results using the relaxed observational errors (see Fig. 1) give more reasonable parameter uncertainties (0.01 – 0.015 dex).

4 DETERMINATION OF $\log g$ FOR AN EXTENDED LIST OF STARS

We apply our grid-based method to an extended list of stars with measured global seismic quantities and atmospheric parameters. Table 3 lists the star name along with the other measured parameters that are used as input observations to our method. The first part of the table comprises primarily bright stars whose oscillation properties have been measured either from ground-based or spaced-based instrumentation (see references given in the table). For most of these stars no errors are cited for $\langle\Delta\nu\rangle$ and $\nu_{\rm max}$. The second part of the table lists a set of 22 solar-type stars observed by the *Kepler* spacecraft and studied in Mathur et al. (2012). We have taken the seismic and atmospheric data directly from this paper. To conduct a homogenous analysis of these stars we adopted a 1.1 μHz error on $\langle\Delta\nu\rangle$ for all of the stars, and a 5% error on $\nu_{\rm max}$, typical of what has been found for the large sample of *Kepler* stars (see Huber et al. 2011 and Sect. 5.1).

Table 4 lists the derived value of $\log g$ and 2σ uncertainties for each of the stars using RadEx10. We show two values of $\log g$; the first is obtained by using the four input constraints $\{\langle\Delta\nu\rangle,\nu_{\rm max},T_{\rm eff},[{\rm Fe/H}]\}$ and the second $\log g_{\rm no[Fe/H]}$ is obtained by omitting [Fe/H] from the analysis.

Figure 3 top panel compares the derived values of $\log g$ for the *Kepler* stars with those determined using the individual oscillation frequencies, as given by Mathur et al. (2012), with the 1σ error bars overplotted. We see that the grid-based method provides $\log g$ consistent with those derived from a detailed asteroseismic analysis, although a very small

Table 3. Measured seismic and atmospheric properties for an extended list of Sun-like oscillators

Star Name	$\langle\Delta\nu\rangle$ (μHz)	$\nu_{\rm max}$ (μHz)	$T_{\rm eff}$ (K)	[Fe/H] (dex)
HD 10700	169.0[a]	4500[a]	5383 ± 47[a]	-0.10 ± 0.07
HD 17051	120.0[b]	2700[b]	6080 ± 80	0.15 ± 0.07
HD 23249	43.8[c]	700[c]	4986 ± 57[d]	0.15 ± 0.07
HD 49385	55.8[s]	1013[s]	6095 ± 65[s]	+0.09 ± 0.05[s]
HD 52265	98.3 ± 0.1[l]	1800[l]	6100 ± 60[l]	0.19 ± 0.05[l]
HD 61421	55.0	1000	6494 ± 48	0.01 ± 0.07
HD 63077	97.0[e]	2050[e]	5710 ± 80	-0.86 ± 0.07
HD 102870	72.1[f]	1400[f]	6012 ± 64[g]	0.12 ± 0.07
HD 121370	39.9[h]	750[h]	6028 ± 47[d]	0.24 ± 0.07
HD 139211	85.0[e]	1800[e]	6200 ± 80	-0.04 ± 0.07
HD 160691	90.0[i]	2000[i]	5665 ± 80	0.32 ± 0.07
HD 165341	161.7[j]	4500[j]	5300 ± 80	0.12 ± 0.07
HD 170987	55.5 ± 0.8[m]	1000[m]	6540 ± 100[m]	-0.15 ± 0.06[m]
HD 181420	75.0[n]	1500 ± 300[n]	6580 ± 105[o]	0.00 ± 0.06[o]
HD 181906	87.5 ± 2.6[p]	1912 ± 47[p]	6300 ± 150[p]	-0.11 ± 0.14[p]
HD 186408	103.1[q]	2150[q]	5825 ± 50[q]	0.01 ± 0.03[q]
HD 186427	117.2[q]	2550[q]	5750 ± 50[q]	0.05 ± 0.02[q]
HD 185395	84.0[r]	2000[r]	6745 ± 150[r]	-0.04[r]
HD 203608	120.4[k]	2600[k]	5990 ± 80	-0.74 ± 0.07
HD 210302	89.5[e]	1950[e]	6235 ± 80	0.01 ± 0.07
KIC 3632418	60.63 ± 0.37	1110 ± 20	6150 ± 70	-0.19 ± 0.07
KIC 3656476	93.70 ± 0.22	1940 ± 25	5700 ± 70	0.32 ± 0.07
KIC 4914923	88.61 ± 0.32	1835 ± 60	5840 ± 70	0.14 ± 0.07
KIC 5184732	95.53 ± 0.26	2070 ± 20	5825 ± 70	0.39 ± 0.07
KIC 5512589	68.52 ± 0.33	1240 ± 25	5710 ± 70	0.04 ± 0.07
KIC 6106415	103.82 ± 0.29	2285 ± 20	5950 ± 70	-0.11 ± 0.07
KIC 6116048	100.14 ± 0.22	2120 ± 20	5895 ± 70	-0.26 ± 0.07
KIC 6603624	110.28 ± 0.25	2405 ± 50	5600 ± 70	0.26 ± 0.07
KIC 6933899	72.15 ± 0.25	1370 ± 30	5830 ± 70	-0.01 ± 0.07
KIC 7680114	85.13 ± 0.14	1660 ± 25	5815 ± 70	0.10 ± 0.07
KIC 7976303	50.95 ± 0.37	910 ± 25	6050 ± 70	-0.52 ± 0.07
KIC 8006161	148.21 ± 0.19	3545 ± 140	5340 ± 70	0.38 ± 0.07
KIC 8228742	63.15 ± 0.32	1160 ± 40	6000 ± 70	-0.15 ± 0.07
KIC 8379927	120.86 ± 0.43	2880 ± 65	5960 ± 125	-0.30 ± 0.07
KIC 8760414	116.24 ± 0.56	2510 ± 95	5765 ± 70	-1.19 ± 0.07
KIC 10018963	55.99 ± 0.35	985 ± 10	6300 ± 65	-0.47 ± 0.50
KIC 10516096	84.15 ± 0.36	1710 ± 15	5900 ± 70	-0.10 ± 0.07
KIC 10963065	103.61 ± 0.41	2160 ± 35	6015 ± 70	-0.21 ± 0.07
KIC 11244118	71.68 ± 0.16	1405 ± 20	5705 ± 70	0.34 ± 0.07
KIC 11713510	69.22 ± 0.20	1235 ± 15	5930 ± 52	...
KIC 12009504	88.10 ± 0.42	1825 ± 20	6060 ± 70	-0.09 ± 0.07
KIC 12258514	74.75 ± 0.23	1475 ± 30	5950 ± 70	0.02 ± 0.07

References: All HD star measurements without references are taken from Bruntt et al. (2010), [a]Teixeira et al. (2009), [b]Vauclair et al. (2008), [c]Bouchy & Carrier (2003), [d]Thévenin et al. (2005), [e]Bruntt et al. (2010), [f]Carrier et al. (2005), [g]North et al. (2009), [h]Carrier et al. (2005), [i]Bouchy et al. (2005), [j]Carrier & Eggenberger (2006), [k]Mosser et al. (2008), [l]Ballot et al. (2011) [m]Mathur et al. (2010) [n]Barban et al. (2009) [o]Bruntt (2009) [p]García et al. (2009) [q]Metcalfe et al. (2012b)[r]Guzik et al. (2011) [s]Deheuvels et al. (2010) Where $\langle\Delta\nu\rangle$ is not explicitly given it is calculated from the highest amplitude $l = 0$ modes. Values for the KIC stars are taken from Mathur et al. (2012).

trend can be seen. For some of their stars they obtain a fitted He abundance of $Y_0 = 0.22$, i.e. sub-Big Bang values, and at the edge of their searched parameter space. The corresponding fitted mass and radius may then be slightly skewed. If we omit these stars, then we fit a slope of 0.07 ± 0.02 to the difference between the their and our $\log g$ values, implying that the trend is not statistically significant. Silva Aguirre et al. (2012) have analysed 6 of these stars and the lower panel of Fig. 3 shows a comparison between their $\log g$ values with ours. Fitting the differences between our results, we obtain a slope of –0.0004 ± 0.0249 with a systematic offset of -0.005 ± 0.010, indicating no systematic trends.

5 PRECISION IN $\log g$ FOR A LARGE SAMPLE OF *Kepler* STARS OF CLASSES IV/V

Our primary objective was to test the accuracy of a seismic $\log g$ by using bright nearby targets that have independent mass and radius measurements. We showed in Sect. 3.4 (see Fig. 1) that our accuracy should be on a level of 0.01 dex,

Table 4. Derived seismic $\log g$ for an extended list of Sun-like oscillators. $\log g$ and $\log g_{\rm no[Fe/H]}$ refer to using $\{\langle\Delta\nu\rangle, \nu_{\rm max}, T_{\rm eff}, {\rm [Fe/H]}\}$ and $\{\langle\Delta\nu\rangle, \nu_{\rm max}, T_{\rm eff}\}$ as the constraints in the analysis. For a homogenous analysis we adopted 1.1 μHz and 5% as the errors on $\langle\Delta\nu\rangle$ and $\nu_{\rm max}$. We list 2σ uncertainties for $\log g$.

Star Name	$\log g$ (dex)	$\log g_{\rm no[Fe/H]}$ (dex)
HD 10700	4.55 ± 0.02	4.57 ± 0.02
HD 17051	4.40 ± 0.02	4.39 ± 0.03
HD 23249	3.81 ± 0.02	3.78 ± 0.04
HD 49385	3.98 ± 0.02	3.97 ± 0.04
HD 52265	4.28 ± 0.02	4.24 ± 0.02
HD 61421	3.98 ± 0.02	3.97 ± 0.03
HD 63077	4.22 ± 0.02	4.25 ± 0.03
HD 102870	4.11 ± 0.02	4.10 ± 0.04
HD 121370	3.82 ± 0.03	3.82 ± 0.03
HD 139211	4.20 ± 0.02	4.21 ± 0.02
HD 160691	4.22 ± 0.02	4.21 ± 0.02
HD 165341	4.54 ± 0.02	4.54 ± 0.02
HD 170987	3.98 ± 0.02	3.98 ± 0.03
HD 181420	4.15 ± 0.02	4.15 ± 0.03
HD 181906	4.22 ± 0.02	4.23 ± 0.02
HD 186408	4.28 ± 0.02	4.28 ± 0.03
HD 186427	4.36 ± 0.02	4.35 ± 0.03
HD 185395	4.22 ± 0.02	4.23 ± 0.02
HD 203608	4.35 ± 0.02	4.37 ± 0.04
HD 210302	4.23 ± 0.02	4.24 ± 0.03
KIC 3632418	4.00 ± 0.03	4.01 ± 0.04
KIC 3656476	4.23 ± 0.02	4.23 ± 0.03
KIC 4914923	4.21 ± 0.02	4.21 ± 0.03
KIC 5184732	4.26 ± 0.02	4.25 ± 0.02
KIC 5512589	4.05 ± 0.02	4.04 ± 0.04
KIC 6106415	4.29 ± 0.02	4.30 ± 0.03
KIC 6116048	4.25 ± 0.02	4.27 ± 0.03
KIC 6603624	4.32 ± 0.02	4.32 ± 0.02
KIC 6933899	4.09 ± 0.02	4.09 ± 0.04
KIC 7680114	4.18 ± 0.02	4.17 ± 0.04
KIC 7976303	3.89 ± 0.02	3.92 ± 0.04
KIC 8006161	4.48 ± 0.02	4.48 ± 0.02
KIC 8228742	4.02 ± 0.03	4.02 ± 0.04
KIC 8379927	4.36 ± 0.02	4.40 ± 0.02
KIC 8760414	4.31 ± 0.02	4.35 ± 0.03
KIC 10018963	3.96 ± 0.03	3.96 ± 0.03
KIC 10516096	4.17 ± 0.02	4.18 ± 0.03
KIC 10963065	4.28 ± 0.02	4.29 ± 0.04
KIC 11244118	4.09 ± 0.02	4.08 ± 0.03
KIC 11713510	4.05 ± 0.04	4.05 ± 0.03
KIC 12009504	4.21 ± 0.02	4.21 ± 0.03
KIC 12258514	4.12 ± 0.02	4.12 ± 0.03

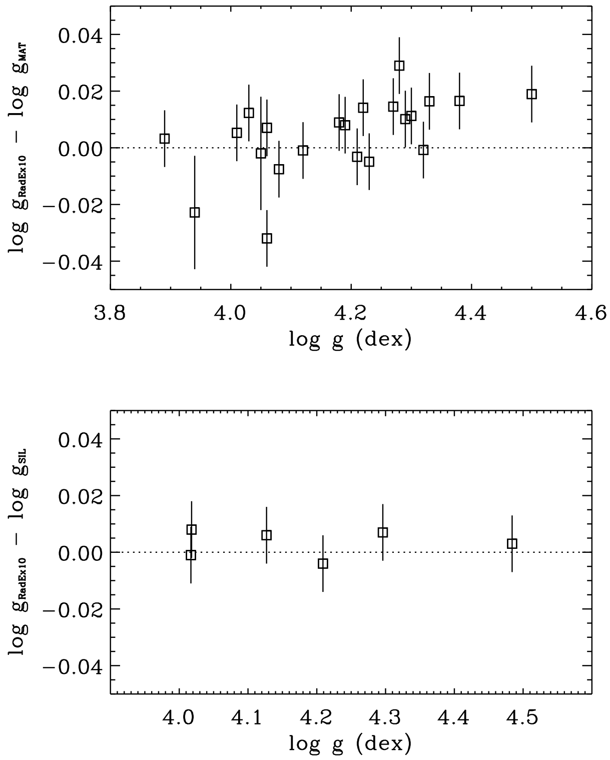

Figure 3. Comparison of $\log g$ derived by RadEx10 with (top) a detailed seismic analyses (Mathur et al. 2012) for 22 Sun-like stars observed by *Kepler*, and (bottom) six common stars with Silva Aguirre et al. (2012).

within 1σ of the derived uncertainty, using either the sets $\{\langle\Delta\nu\rangle, \nu_{\rm max}, T_{\rm eff}, {\rm [Fe/H]}\}$ or $\{\langle\Delta\nu\rangle, \nu_{\rm max}, T_{\rm eff}\}$ for the small sample of stars covering the range $3.9 < \log g < 4.6$. In this section we investigate the *precision in* $\log g$ for a sample of 403 V/IV stars ($\log g > 3.75$) observed with the *Kepler* spacecraft by employing the same analysis methods. In particular we pay attention to systematic errors by 1) using different sets of observational constraints, 2) comparing results using two different methods which incorporate different stellar evolution codes and physics, and 3) we also show the distribution of errors as a function of magnitude and $\log g$ and summarize the uncertainties and systematics as a function of magnitude.

5.1 Observations

During the first 9 months of the *Kepler* mission targets to be monitored with a 1 minute cadence during 1 month each were selected by the KASC[5]. These stars were chosen based on information available in the *Kepler Input Catalog*, KIC, (Brown et al. 2011) and were expected to exhibit solar-like oscillations. A total of 588 stars with values of $\log g$ between 3.0 and 4.5 dex were analysed (García et al. 2011) and had their global seismic quantities determined (Huber et al. 2011; Verner et al. 2011; Chaplin et al. 2011). In this paper we concentrate on a subset of 403 less-evolved stars with derived $\log g$ between 3.75 and 4.50 dex, the range for which we have validated our methods.

The global seismic quantities have been determined using the SYD pipeline as described by Huber et al. (2009) (Chaplin. et al. in prep.). The uncertainties on the seismic quantities include a contribution from the scatter between different analysis pipelines (Verner et al. 2011, Chaplin et al. in prep.). We note that this pipeline uses the reference values of $\langle\Delta\nu\rangle_\odot = 135.1$ μHz and $\nu_{\rm max\odot} = 3{,}090$ μHz. We

[5] *Kepler* Asteroseismic Science Consortium, see `http://astro.phys.au.dk/KASC/`

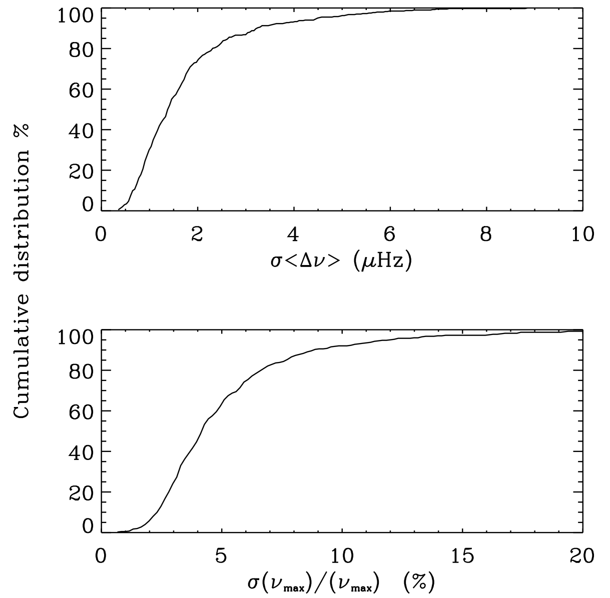

Figure 4. Cumulative distributions of the errors in $\langle\Delta\nu\rangle$ (top) and $\nu_{\rm max}$ (bottom).

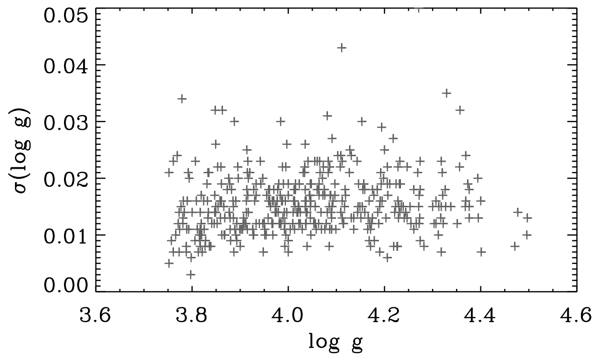

Figure 5. Distribution of uncertainties in $\log g$ as a function of $\log g$ for a sample of 403 *Kepler* stars, using RadEx10 with observational constraints comprising $\{T_{\rm eff}, \langle\Delta\nu\rangle, \nu_{\rm max}\}$.

adopted these values in our grid of models to avoid possible systematic errors. Figure 4 shows the cumulative distribution for the errors in the seismic observations, $\langle\Delta\nu\rangle$ (continuous) and $\nu_{\rm max}$(dashed) in units of μHz and %, respectively, for the 403 stars. Our choice for absolute and relative errors is for consistency with units used in the recent literature. We show the cumulative distribution of the errors in order to see the typical errors for 50% and 80% of the sample, which justifies the errors that we used in Sect. 3.3. These are less than 1.1/2.0 μHz for $\langle\Delta\nu\rangle$, and less than 5%/8% for $\nu_{\rm max}$, respectively.

The $T_{\rm eff}$ derived by the KIC have been shown not to be accurate on a star-to-star basis (Molenda-Żakowicz et al. 2011), and so the ground-based *Kepler* support photometry (Brown et al. 2011) was re-analysed by Pinsonneault et al. (2012) to determine more accurate $T_{\rm eff}$ for the ensemble of *Kepler* stars. These are the temperatures that we adopt for our first analysis and we refer to them as $T_{\rm eff\,Pin}$. In their work they consider a mean [Fe/H] = – 0.20 ± 0.30 dex for all of the stars. Silva Aguirre et al. (2012) adapt an infrared flux method presented by Casagrande et al. (2010) for determining stellar temperatures. In their work they apply this method to the large ensemble of *Kepler* stars to provide an alternative determination of $T_{\rm eff}$. We also adopt their $T_{\rm eff}$ determinations in order to study the effect of biases in temperature estimates on the derived value of $\log g$. We refer to these temperature estimates as $T_{\rm eff\,irfm}$. Support spectroscopic data have also been obtained for 93 of the stars and the metallicities are presented in Bruntt et al. (2012). We further include these data to study the effects of possible biases arising from lack/inclusion of metallicity information.

5.2 $\log g$ determined by using different sets of observations

Using our validated method described in Sect. 3.2, we calculated values of $\log g$ and their uncertainties for the sample of 403 stars using the set of observations comprising $\{T_{\rm eff\,Pin}, \langle\Delta\nu\rangle, \nu_{\rm max}\}$ while adopting a mean [Fe/H] = – 0.20 ± 0.30 dex. We refer to this set as the reference set. The distribution of the uncertainties as a function of $\log g$ is shown in Figure 5. Here it can be seen that typical uncertainties in $\log g$ for this set of 403 *Kepler* stars is below 0.02 dex (there is one star with an error of 0.05 dex), with a mean value of 0.015 dex.

In Figure 6 we show the difference in the fitted $\log g$ while considering different input observational sets compared to the reference set 'log g$_{\rm ref}$'. The subsets are: Set 1 which considers $\langle\Delta\nu\rangle$ and $T_{\rm eff\,Pin}$ only and Set 2 which considers $\langle\Delta\nu\rangle$, $\nu_{\rm max}$, and $T_{\rm eff\,irfm}$. We note that for all of the analyses [Fe/H] was constrained to –0.20 ± 0.30 dex, which corresponds to >90% of the models of the grid.

Inspecting the top panel of Fig. 6 (Set 1) one can see that by omitting $\nu_{\rm max}$ as an observed quantity can result in differences of over 0.05 dex for a very small percentage of the stars, but the absolute difference between the full set of results is +0.005 dex with an rms of 0.01 dex. The uncertainties also increase by $\sim$ 0.01 dex, which allows for the extra scatter.

Inspecting the lower panel of Fig. 6 (Set 2) one can see that the $T_{\rm eff}$ derived by using different photometric scales results in a mean difference in $\log g$ of -0.002 dex (i.e. no significant overall effect) with an rms scatter of 0.007 dex. This latter fact implies that we can expect to add just under 0.01 dex to the error budget in $\log g$ by considering $T_{\rm eff}$ derived from different methods. We found a similar result in Sect. 3.5 for β Hydri.

The mean uncertainties in $\log g$ for Set 1 and 2 are 0.023 and 0.015 dex, respectively, while those for the reference set are 0.015 dex. The accuracy of these $\log g$ (if we consider the reference set to be correct) is within 1σ.

Figure 7 compares the derived $\log g$ using the reference set of observations, to those with measured $T_{\rm eff}$ and [Fe/H] from Bruntt et al. (2012). The absolute mean residual is 0.002 dex and is highlighted by the dotted grey line.

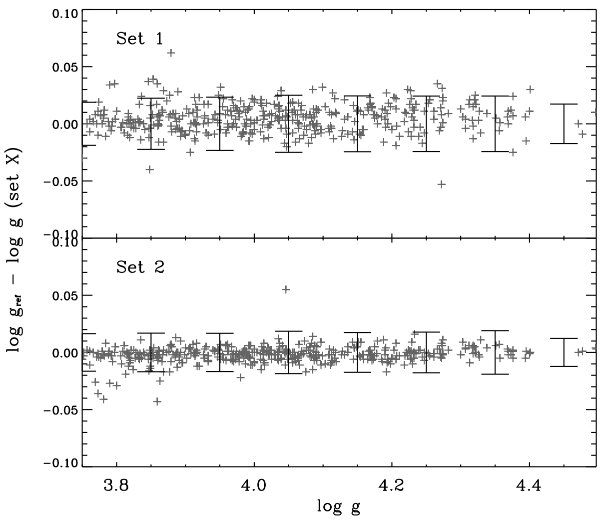

Figure 6. Differences in $\log g$ using subsets of observational constraints. The reference set comprise ($\langle\Delta\nu\rangle$, $\nu_{\rm max}$, $T_{\rm eff\,Pin}$). Set 1 and 2 comprise ($\langle\Delta\nu\rangle$, $T_{\rm eff\,Pin}$) and ($\langle\Delta\nu\rangle$, $\nu_{\rm max}$, $T_{\rm eff\,IR}$), respectively. For all sets [Fe/H] = –0.20 dex. The error bars are average error bars measured over bins of 0.1 dex.

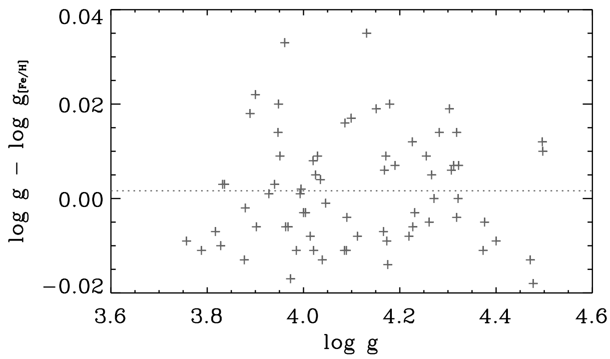

Figure 7. Differences in $\log g$ derived when we adopt [Fe/H] = –0.20 ± 0.30 dex for all of the stars with the metallicities derived from spectroscopic analysis by Bruntt et al. (2012).

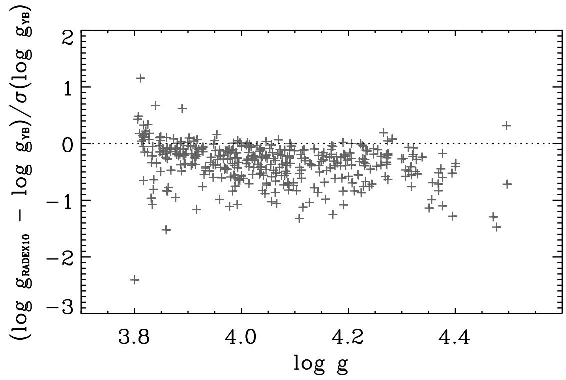

Figure 8. The difference between the values of $\log g$ obtained by RadEx10 and Yale-Bham as a function of $\log g$ and normalised by the Yale-Bham errors.

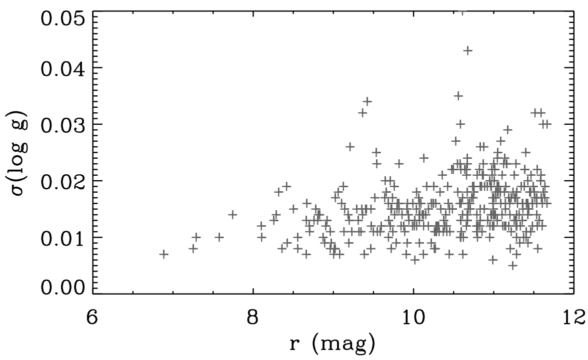

Figure 9. Distribution of errors in $\log g$ for 588 *Kepler* V/IV stars as a function of r magnitude.

However, $\log g$ can differ by up to 0.02 dex because of the constraint on [Fe/H]. This 0.02 dex is also consistent with what we found in Sect. 3.5 for β Hydri when we considered different metallicity constraints.

5.3 Comparison of results using different codes

To investigate the possible source of systematics arising from using a different evolution code and input physics, we determined $\log g$ using a second pipeline code, Yale-Bham (Gai et al. 2011; Creevey et al. 2012a). Details of the code can be found in the cited papers. Here, it suffices to know that the method is very similar to that of RadEx10, but the evolution code is based on YREC (Demarque et al. 2008) in its non-rotating configuration, with the following specifications: OPAL EOS (Rogers & Nayfonov 2002) and OPAL high-temperature opacitites (Iglesias & Rogers 1996) supplemented with low-temperature opacitites from Ferguson et al. (2005), and the NACRE nuclear reaction rates (Angulo et al. 1999). Diffusion of helium and heavy-elements were included, unlike RadEx10.

Figure 8 shows the difference in the derived value of $\log g$ between RadEx10 and Yale-Bham using $\{\langle\Delta\nu\rangle$,$\nu_{\rm max}$,$T_{\rm eff\,Pin}$,[Fe/H]=–0.2$\}$. We show the normalised difference, i.e. divided by the Yale-Bham errors, which are very similar to the RadEx10 errors. As can be seen from Fig. 8 the agreement in $\log g$ between the different methods is within 1σ or < 0.01 dex for 98% of the stars and 2σ for all stars except one. A small absolute difference of 0.005 dex is found with a standard deviation of 0.005 dex. This is most likely due to the different physics adopted in the codes. A very slight systematic trend is present, but is insignificant. The slope is -0.005 ± 0.005 dex. The agreement between the results using the different codes and methods is very encouraging. We can consider an upper limit of 0.01 dex as a typical systematic error arising from different employed codes.

Table 5. Summary of uncertainties $\langle\sigma\rangle$ and systematic errors in $\log g$ expected from the *Kepler* sample of stars as a function of magnitude. The systematic errors have subscripts which refer to possible sources of errors in the input $T_{\rm eff}$, [Fe/H], and the code that is used to generate the stellar models (see Sects. 5.2 and 5.3 for details).

r (mag)	$\langle\sigma\rangle$ (dex)	$\langle\sigma_{\rm Teff}\rangle$ (dex)	$\langle\sigma_{\rm [Fe/H]}\rangle$ (dex)	$\langle\sigma_{\rm code}\rangle$ (dex)
<9	0.012	0.004	0.014	0.005
$9 < r < 10$	0.014	0.004	0.009	0.004
$10 < r < 11$	0.016	0.009	...	0.006
$11 < r < 12$	0.017	0.009	...	0.006

5.4 Precision in $\log g$ as a function of magnitude

In Figure 9 we show the typical uncertainties in $\log g$ as a function of SDDS r magnitude (obtained from the KIC) while using the reference set of observations. As expected, Fig. 9 shows that precision improves with apparent brightness, where the measurements are much more reliable, and hence have smaller errors. In general, we can expect typical uncertainties in $\log g$ of less than 0.03 dex for all stars with r magnitudes less than 12.

5.5 Summary of results for the sample of *Kepler* stars

Considering the results for the *Kepler* data presented here, we conclude that the *Kepler* stars give a mean precision of between 0.01 and 0.02 dex (max 0.03 dex for 99% of stars) in $\log g$ for $3.75 < \log g < 4.50$ when $\langle\Delta\nu\rangle$, $\nu_{\rm max}$, and $T_{\rm eff}$ are used as the input constraints for the pipeline anaysis. A typical systematic error of no more than 0.01 dex can be added to account for a possible systematic error in $T_{\rm eff}$, such as that obtained by applying different calibration methods to photometry. Similarly, we can add a systematic error of 0.02 dex due to an incorrect or lack of a [Fe/H] measurement. We also showed that using different models and physics in the pipeline analyses yields results in $\log g$ consistent to within 0.01 dex i.e. almost no model dependence. This gives an upper limit of 0.04 dex to account for systematic errors. In Table 5 we summarize this information while taking into account the observed magnitude of the star.

Eliminating one of the seismic indices from the set of data yields a zero offset in the results for the full sample of stars, although differences of over 0.05 dex were found for < 1% of the stars, and a typical scatter of 0.02 dex was evident. However, the uncertainties also increased by 0.01 dex.

6 DISCUSSION

The first objective of this paper was to investigate if we can determine $\log g$ reliably using global seismic quantities and atmospheric data. We showed that our method is reliable by comparing our results with values of $\log g$ derived from direct mass and radius estimates of bright nearby stars. We then applied our method to a list of 41 Sun-like stars and derived $\log g$ to within 1σ of those from Mathur et al. (2012). We also showed that for a sample of 400+ *Kepler* stars (6< r mag < 12) with $\log g$ between 3.75 and 4.50 typical uncertainties of less than 0.02 dex can be expected and we estimated systematic errors of no more than 0.04 dex arising from errors in $T_{\rm eff}$ and [Fe/H] measurements and using different codes.

All of the *Kepler* stars will be observed by the Gaia mission, and for this reason they provide a valid set of calibration stars, by constraining $\log g$ with precisions and accuracies much better than spectroscopic or isochrone methods provide for the current list of calibration stars for Gaia. The astrophysical parameters to be determined from Gaia data using the astrometry, photometry and BP/RP spectrophotometry are $T_{\rm eff}$, $A_{\rm G}$, [Fe/H], and $\log g$. By ensuring that the `GSP_Phot` methods deliver $\log g$ consistent with the seismic value will reduce the uncertainties and inaccurcies in the other parameters. Moreover, an independent $\log g$ provides an extra constraint for the determination of the atmospheric parameters from `GSP_Spec` where degeneracies between $T_{\rm eff}$ and $\log g$ severely inhibit the precision of atmospherically extracted parameters and chemical abundances.

While in this paper we concentrated primarily on using *Kepler* data to determine $\log g$, we note that both the *Kepler* and CoRoT fields have great potential in other aspects. For example, Silva Aguirre et al. (2012) develop a method which couples asteroseismic analyses with the infrared flux method to determine stellar parameters including effective temperatures and bolometric fluxes, and hence distances. Miglio et al. (2012) and Miglio et al. (2012b) determine distances, masses, and ages of red giants from the CoRoT fields to constrain galactic evolution models. The distances obtained by both Silva Aguirre et al. (2012) and Miglio et al. (2012b) can be compared directly with a Gaia distance for either calibration of Gaia data or stellar models. By combining data from *Kepler* and CoRoT with Gaia data we can also determine extremely precise angular diameters by coupling a seismically determined radius with the Gaia parallax. Finally, these stars will also be excellent calibrators for the FLAME workpackage of Gaia, which aims to determine masses, radii, and ages for all of the Gaia stars.

7 CONCLUSION

In this work we explored the use of F, G, K IV/V stars observed in the *Kepler* field as a possible source of calibration stars for fundamental stellar parameters from the Gaia mission. Our first objective was to test the reliability/accuracy of a seismically determined $\log g$, and using a sample of seven bright nearby targets we proved that seismic methods are accurate (see Fig. 1) by obtaining results to within 1σ of the currently accepted $\log g$ values. We showed, however, that the accuracy of the input atmospheric parameters does play a role in the accuracy of the derived parameters. For β Hydri we found that errors in the atmospheric parameters, and in particular [Fe/H], can change $\log g$ by 0.02 dex.

We then applied our grid-based method RadEx10 to an extended sample of stars from the literature. We derived their seismic $\log g$ and these are given in Table 4. We showed that a grid-based $\log g$ is consistent with the values of $\log g$ obtained by detailed seismic analysis from Mathur et al. (2012) and in excellent agreement with the results from Silva Aguirre et al. (2012) for the 6 common stars. We find typical precisions in $\log g = 0.02$ dex.

We finally studied the distribution of errors in $\log g$ as derived by two analyses methods for a sample of 403 *Kepler* stars with $3.75 < \log g < 4.5$, and we concluded that we can expect a typical uncertainty of between 0.01 and 0.02 dex in $\log g$ for F, G, K IV/V stars (see Table 5). We can add a total of 0.04 dex as a systematic error which arises from the adopted temperature scales (0.01 dex) and measured metallicities (0.02 dex) as well as the grids of models used (0.01 dex), which differ in evolution codes and input physics. The precisions in the data are unprecedented, and the systematic errors are much smaller than those stemming from any other method, especially for $7 < V < 12$ stars (see e.g. Creevey et al. 2012a Fig 1 and Table 3 which compare spectroscopically derived $\log g$ for five *Kepler* stars with $V \sim 11$).

As a final remark, we highlight that while there are >500 IV/V stars in *Kepler* field and some in CoRoT field that exhibit Sun-like oscillations, there are also 1000's of red giants in both CoRoT and *Kepler* fields with these same measured quantities, however, the accuracy of these star's seismic $\log g$ is yet to be shown.

ACKNOWLEDGEMENTS

OLC thanks Daniel Huber, Luca Casagrande, and Victor Silva Aguirre for making data available. SB acknowledges NSF grant AST-1105930. AMS is partially supported by the European Union International Reintegration Grant PIRG-GA-2009-247732, the MICINN grant AYA2011-24704, by the ESF EUROCORES Program EuroGENESIS (MICINN grant EUI2009-04170), by SGR grants of the Generalitat de Catalunya and by the EU-FEDER funds. OLC is a Henri Poincaré Fellow at the Observatoire de la Côte d'Azur, partially funded by Conseil Général des Alpes-Maritimes.

REFERENCES

Allende Prieto C., Asplund M., García López R. J., Lambert D. L., 2002, ApJ, 567, 544
Angulo C. et al., 1999, Nuclear Physics A, 656, 3
Bahcall J. N., Pinsonneault M. H., 1992, ApJL, 395, L119
Bailer-Jones C. A. L., 2010, MNRAS, 403, 96
Ballot J. et al., 2011, A&A, 530, A97
Barban C. et al., 2009, A&A, 506, 51
Barbuy B. et al., 2003, ApJ, 588, 1072
Basu S., Chaplin W. J., Elsworth Y., 2010, ApJ, 710, 1596
Baudin F. et al., 2011, A&A, 529, A84
Bazot M. et al., 2011, A&A, 526, L4
Bedding T. R., 2011, ArXiv e-prints
Bedding T. R. et al., 2010, ApJL, 713, L176
Bedding T. R., Kjeldsen H., 2003, PASA, 20, 203
Bedding T. R., Kjeldsen H., Arentoft T., Bouchy F., Brandbyge J., Brewer B. J., Butler R. P., Christensen-Dalsgaard J., 2007, ApJ, 663, 1315
Benomar O. et al., 2009, A&A, 507, L13
Bigot L., Kervella P., Thévenin F., Ségransan D., 2006, A&A, 446, 635
Bigot L., Mourard D., Berio P., Thévenin F., Ligi R., Tallon-Bosc I., Chesneau O., Delaa O., 2011, A&A, 534, L3
Bijaoui A., Recio-Blanco A., de Laverny P., Ordenovic C., 2010, in ADA 6 - Sixth Conference on Astronomical Data Analysis.
Böhm-Vitense E., 1958, Zeitschrift für Astrophysik, 46, 108
Bonaca A. et al., 2012, ApJL, 755, L12
Borucki W. J. et al., 2010, Science, 327, 977
Bouchy F., Bazot M., Santos N. C., Vauclair S., Sosnowska D., 2005, A&A, 440, 609
Bouchy F., Carrier F., 2002, A&A, 390, 205
Bouchy F., Carrier F., 2003, ApSS, 284, 21
Boyajian T. S. et al., 2012, ApJ, 746, 101
Brandão I. M. et al., 2011, A&A, 527, A37
Brown T. M., Gilliland R. L., 1994, ARAA, 32, 37
Brown T. M., Latham D. W., Everett M. E., Esquerdo G. A., 2011, Astronomical Journal, 142, 112
Bruntt H., 2009, A&A, 506, 235
Bruntt H. et al., 2012, MNRAS, 423, 122
Bruntt H. et al., 2010, MNRAS, 405, 1907
Carrier F., Eggenberger P., 2006, A&A, 450, 695
Carrier F., Eggenberger P., Bouchy F., 2005, A&A, 434, 1085
Carrier F., Eggenberger P., D'Alessandro A., Weber L., 2005, New Astronomy, 10, 315
Casagrande L., Ramírez I., Meléndez J., Bessell M., Asplund M., 2010, A&A, 512, A54
Chaplin W. J. et al., 2011, Science, 332, 213
Christensen-Dalsgaard J., 2008, ApSS, 316, 13
Creevey O. L., Bazot M., 2011, Journal of Physics Conference Series, 271, 012038
Creevey O. L. et al., 2005, ApJL, 625, L127
Creevey O. L. et al., 2012a, A&A, 537, A111
Creevey O. L., Metcalfe T. S., Brown T. M., Jiménez-Reyes S., Belmonte J. A., 2011, ApJ, 733, 38
Creevey O. L., Monteiro M. J. P. F. G., Metcalfe T. S., Brown T. M., Jiménez-Reyes S. J., Belmonte J. A., 2007, ApJ, 659, 616
Creevey O. L., Thévenin F., 2012, in Boissier S., de Laverny P., Nardetto N., Samadi R., Valls-Gabaud D., Wozniak H., eds, SF2A-2012: Proceedings of the Annual meeting of the French Society of Astronomy and Astrophysics. pp 189–193
Creevey O. L. et al., 2012b, A&A, 545, A17
da Silva L. et al., 2006, A&A, 458, 609
Deheuvels S. et al., 2010, A&A, 515, A87
Demarque P., Guenther D. B., Li L. H., Mazumdar A., Straka C. W., 2008, ApSS, 316, 31
Doğan G., Brandão I. M., Bedding T. R., Christensen-Dalsgaard J., Cunha M. S., Kjeldsen H., 2010, ApSS, 328, 101
Eggenberger P., Carrier F., Bouchy F., Blecha A., 2004, A&A, 422, 247
Eggleton P. P., Faulkner J., Flannery B. P., 1973, A&A, 23, 325
Fabbian D., Moreno-Insertis F., Khomenko E., Nordlund Å., 2012, A&A, 548, A35
Ferguson J. W., Alexander D. R., Allard F., Barman T., Bodnarik J. G., Hauschildt P. H., Heffner-Wong A., Tamanai A., 2005, ApJ, 623, 585

Fernandes J., Monteiro M. J. P. F. G., 2003, A&A, 399, 243
Fuhrmann K., Pfeiffer M., Frank C., Reetz J., Gehren T., 1997, A&A, 323, 909
Gai N., Basu S., Chaplin W. J., Elsworth Y., 2011, ApJ, 730, 63
García R. A. et al., 2011, MNRAS, 414, L6
García R. A., Mathur S., Salabert D., Ballot J., Régulo C., Metcalfe T. S., Baglin A., 2010, Science, 329, 1032
García R. A. et al., 2009, A&A, 506, 41
Girard T. M. et al., 2000, Astronomical Journal, 119, 2428
Grevesse N., Noels A., 1993, in Prantzos N., Vangioni-Flam E., Casse M., eds, Origin and Evolution of the Elements. pp 15–25
Grevesse N., Sauval A. J., 1998, Space Sci. Rev., 85, 161
Gruberbauer M., Kallinger T., Weiss W. W., Guenther D. B., 2009, A&A, 506, 1043
Guzik J. A. et al., 2011, ArXiv e-prints
Hekker S. et al., 2009, A&A, 506, 465
Hełminiak K. G. et al., 2012, MNRAS, 425, 1245
Huber D. et al., 2011, ApJ, 743, 143
Huber D. et al., 2012, ApJ, 760, 32
Huber D., Stello D., Bedding T. R., Chaplin W. J., Arentoft T., Quirion P.-O., Kjeldsen H., 2009, Communications in Asteroseismology, 160, 74
Iglesias C. A., Rogers F. J., 1996, ApJ, 464, 943
Kallinger T., Gruberbauer M., Guenther D. B., Fossati L., Weiss W. W., 2010, A&A, 510, A106
Kallinger T. et al., 2010, A&A, 509, A77
Katz D., 2005, in Turon C., O'Flaherty K. S., Perryman M. A. C., eds, ESA Special Publication Vol. 576, The Three-Dimensional Universe with Gaia. p. 51
Kervella P., Thévenin F., Di Folco E., Ségransan D., 2004, A&A, 426, 297
Kervella P., Thévenin F., Morel P., Berthomieu G., Bordé P., Provost J., 2004, A&A, 413, 251
Kervella P., Thévenin F., Ségransan D., Berthomieu G., Lopez B., Morel P., Provost J., 2003, A&A, 404, 1087
Kjeldsen H., Bedding T. R., 1995, A&A, 293, 87
Kjeldsen H. et al., 2005, ApJ, 635, 1281
Lebzelter T. et al., 2012, ArXiv e-prints
Leibacher J. W., Stein R. F., 1971, ApJL, 7, 191
Liu C., Bailer-Jones C. A. L., Sordo R., Vallenari A., Borrachero R., Luri X., Sartoretti P., 2012, ArXiv e-prints
Martić M., Lebrun J.-C., Appourchaux T., Korzennik S. G., 2004, A&A, 418, 295
Mathur S. et al., 2010, A&A, 518, A53
Mathur S. et al., 2012, ApJ, 749, 152
Metcalfe T. S. et al., 2012a, ApJL, 748, L10
Metcalfe T. S. et al., 2012b, ApJL, 748, L10
Metcalfe T. S. et al., 2010, ApJ, 723, 1583
Miglio A. et al., 2012a, MNRAS, 419, 2077
Miglio A. et al., 2012b, ArXiv e-prints
Miglio A., Morel T., Barbieri M., Mosser B., Girardi L., Montalbán J., Valentini M., 2012, in European Physical Journal Web of Conferences. p. 5012
Molenda-Żakowicz J., Latham D. W., Catanzaro G., Frasca A., Quinn S. N., 2011, MNRAS, 412, 1210
Morel T., Miglio A., 2012, MNRAS, 419, L34
Mosser B. et al., 2005, A&A, 431, L13
Mosser B., Deheuvels S., Michel E., Thévenin F., Dupret M. A., Samadi R., Barban C., Goupil M. J., 2008, A&A, 488, 635
Mosser B. et al., 2012, A&A, 537, A30
North J. R. et al., 2007, MNRAS, 380, L80
North J. R. et al., 2009, MNRAS, 393, 245
Perryman M. A. C. et al., 1997, A&A, 323, L49
Pinsonneault M. H., An D., Molenda-Żakowicz J., Chaplin W. J., Metcalfe T. S., Bruntt H., 2012, ApJS, 199, 30
Porto de Mello G. F., Lyra W., Keller G. R., 2008, A&A, 488, 653
Pourbaix D. et al., 2002, A&A, 386, 280
Quirion P.-O., Christensen-Dalsgaard J., Arentoft T., 2010, ApJ, 725, 2176
Recio-Blanco A., Bijaoui A., de Laverny P., 2006, MNRAS, 370, 141
Ribas I., Jordi C., Vilardell F., Fitzpatrick E. L., Hilditch R. W., Guinan E. F., 2005, ApJL, 635, L37
Rogers F. J., Nayfonov A., 2002, ApJ, 576, 1064
Salabert D. et al., 2002, A&A, 390, 717
Salabert D., Régulo C., Ballot J., García R. A., Mathur S., 2011, A&A, 530, A127
Silva Aguirre V. et al., 2012, ApJ, 757, 99
Sousa S. G., Santos N. C., Israelian G., 2012, A&A, 544, A122
Stello D., Bruntt H., Preston H., Buzasi D., 2008, ApJL, 674, L53
Stello D. et al., 2009, ApJ, 700, 1589
Tassoul M., 1980, ApJS, 43, 469
Teixeira T. C. et al., 2009, A&A, 494, 237
Thévenin F., Charbonnel C., de Freitas Pacheco J. A., Idiart T. P., Jasniewicz G., de Laverny P., Plez B., 2001, A&A, 373, 905
Thévenin F., Jasniewicz G., 1992, A&A, 266, 85
Thévenin F., Kervella P., Pichon B., Morel P., di Folco E., Lebreton Y., 2005, A&A, 436, 253
Toutain T., Froehlich C., 1992, A&A, 257, 287
Ulrich R. K., 1970, ApJ, 162, 993
van Leeuwen F., 2007, A&A, 474, 653
Vandakurov Y. V., 1968, Soviet Astronomy, 11, 630
Vauclair S., Laymand M., Bouchy F., Vauclair G., Hui Bon Hoa A., Charpinet S., Bazot M., 2008, A&A, 482, L5
Verner G. A. et al., 2011, MNRAS, 415, 3539
Worley C. C., de Laverny P., Recio-Blanco A., Hill V., Bijaoui A., Ordenovic C., 2012, A&A, 542, A48